RSC Advances

PAPER

View Article Online
View Journal | View Issue

Open Access Article. Published on 17 February 2021. Downloaded on 10/26/2025 9:33:55 PM.
This article is licensed under a Creative Commons Attribution-NonCommercial 3.0 Unported Licence.

Check for updates

Cite this: *RSC Adv.*, 2021, **11**, 7766

Exploration of CH···F & CF···H mediated supramolecular arrangements into fluorinated terphenyls and theoretical prediction of their third-order nonlinear optical response†

Muhammad Adeel,‡*[a] Muhammad Khalid,‡*[b] Malik Aman Ullah,[a] Shabbir Muhammad,[cd] Muhammad Usman Khan,[ef] Muhammad Nawaz Tahir,[g] Ilham Khan,[a] Muhammad Asghar[h] and Khawar Shahzad Mughal[b]

In the present study, three novel fluorinated terphenyl compounds *i.e.*, 2′,4,4″,5′-tetrafluoro-1,1':4′,1″-terphenyl (**1**), 2′,5′-difluoro-1,1':4′,1″-terphenyl (**2**) and 2′,5′-difluro-4,4″-diphenoxy-1,1:4′,1″-terphenyl (**3**) have been synthesized by Suzuki Miyaura method. Single crystal XRD study reveals ð-ð stacking stabilization in molecular packing along with F···H and F···C interactions. This computational quantum chemical exploration was also done by using density functional theory (DFT) methods. The comparison of experimental (SC-XRD) and theoretical (DFT) investigations on structural parameters have been reported which shows reasonable agreements. Hirshfeld surface analysis explores the strength of intermolecular interactions present in the synthesized compounds. A substantial computational analysis of synthesized compounds is done for their optoelectronic and third-order nonlinear optical properties. The third-order NLO study was performed at M06/6-311G* level of theory. A comparative analysis of third-order polarizability of studied compounds is done with that of *para*-nitroaniline (*p*-NA) molecule which is often considered as a prototype NLO molecule. The third-order NLO analysis results suggest that all investigated compounds **1**, **2** and **3** have significant potential as efficient third-order NLO molecules as compared to *p*-NA. The studied compounds **1**, **2** and **3** possess about 13.7 times, 5.2 times and 5.17 times larger third-order polarizability amplitudes than that of *p*-NA (25.45 × 10^{-36} esu) as calculated at same M06/6-311G* levels of theory. Time-dependent density functional theory (TD-DFT) calculations are performed for electronic excitation energies and their oscillator strengths. The studies of frontier molecular orbitals (FMO) analysis, total and partial density of states (DOS) were performed to investigate the intramolecular charge transfer (ICT) process in the entitled compounds.

Received 7th October 2020
Accepted 25th January 2021

DOI: 10.1039/d0ra08528f

rsc.li/rsc-advances

Introduction

In recent years, the demand and production of innovative nonlinear optical materials (NLO) has increased significantly due to their wide spread application in optoelectronic and photonics.[1–4] The wide range applicability of NLO material is attributed to their fascinating photo-physical behavior upon exposure to intense laser light.[5–7] Among all the materials explored for NLO properties, the synthetic organic compounds got enormous contemporary attention due to their speedy response time, greater laser damage threshold, higher photo-electric coefficients, lower dielectric constants, versatility of design and low-cost development.[8–11]

The NLO related properties of organic compounds arise due to strong intramolecular charge transfer (ICT) which originates from a delocalized π-electron framework or a π-conjugated linker between electron donor and acceptor group, generating a push–pull system.[12] This push–pull system containing π-

[a]Institute of Chemical Sciences, Gomal University, Dera Ismail Khan, Khyber Pukhtunkhwa, Pakistan. E-mail: madeel@gu.edu.pk

[b]Department of Chemistry, Khwaja Fareed University of Engineering & Information Technology, Rahim Yar Khan-64200, Pakistan. E-mail: khalid@iq.usp.br; muhammad.khalid@kfueit.edu.pk

[c]Department of Physics, College of Science, King Khalid University, P.O. Box 9004, Abha 61413, Saudi Arabia

[d]Research Center for Advanced Material Science (RCAMS), King Khalid University, P.O. Box 9004, Abha 61413, Saudi Arabia

[e]Department of Chemistry, University of Okara, Okara-56300, Pakistan

[f]Department of Applied Chemistry, Government College University, Faisalabad-38000, Pakistan

[g]Department of Physics, University of Sargodha, Sargodha, Punjab, Pakistan

[h]Department of Physics, Khwaja Fareed University of Engineering & Information Technology, Rahim Yar Khan-64200, Pakistan

† Electronic supplementary information (ESI) available. CCDC 2025097–2025099. For ESI and crystallographic data in CIF or other electronic format see DOI: 10.1039/d0ra08528f

‡ Both authors contributed equally to this work.

© 2021 The Author(s). Published by the Royal Society of Chemistry

Open Access Article. Published on 17 February 2021. Downloaded on 10/26/2025 9:33:55 PM.
This article is licensed under a Creative Commons Attribution-NonCommercial 3.0 Unported Licence.

conjugated organic compounds have emerged as an attractive class of third-order NLO materials due to their potentially broad third-order susceptibilities associated with short turnaround time.[13–15] The third-order NLO response plays a chief role in recent time automated applications. Generally, third-order NLO polarizability is regarded as sign of two photon absorption (TPA).[16] Kamath *et al.* synthesized a range of new chalcones containing terphenyl which demonstrated third order NLO and optical power limiting activity due to two-photon absorption.[17]

Terphenyls are aromatic non-planar structures residing of three phenyl rings chain connected by single bonds. Due to π-conjugated system, terphenyl derivatives and fluorinated terphenyle demonstrate distinctive electronic, optical and bioactive properties.[18–30] The synthesis of terphenyl and fluorinated terphenyls derivatives have been a blooming topic of research due to their wide range of application in drug discovery and material sciences.[31] Several methods and strategies have been established in this regard, but the most general and productive method among them is palladium-catalyzed Suzuki Miyaura coupling method.

Due to limited literature available regarding to the third-order NLO properties of terphenyls, herein this research work, the synthesis of three novel centrosymmetric fluorinated terphenyl compounds *i.e.* 2′,4,4″,5′-tetrafluoro-1,1':4′,1″-terphenyl (**1**), 2′,5′-difluoro-1,1':4′,1″-terphenyl (**2**) and 2′,5′-difluro-4,4″-diphenoxy-1,1:4′,1″-terphenyl (**3**) has been reported through Suzuki Miyaura coupling approach having potential for third-order NLO response. The centrosymmetric crystal groups of all the synthesized compounds prevent any use in second-order NLO applications because compounds with centrosymmetric crystal groups do not show NLO response at bulk-levels.

Experimental and instrumentation

General scheme of synthesis and instrumentation

Analytical grade chemicals (Merck®, Acros®, and Aldrich®) and commercial grade solvent were purchased, which were distilled prior to use. The starting material, 1,4-dibromo-2,5-difluorobenzene was treated with three different aryl boronic acids under Suzuki Miyaura condition in the presence of $Pd(PPh_3)_4$ catalyst, K_3PO_4 base and methanol suspension on a magnetic hot plate for about 8 hours at 90–100 °C (Scheme 1). The general catalytic mechanism completed in three steps *i.e.*, oxidative addition, transmetallation and reductive elemination (Scheme S1†). The product formation was monitored by thin layer chromatography (TLC) followed by purification process through column chromatography. Ethyl acetate/hexane mixture was used as a solvent front and eluting system in both cases. The compounds were further characterized by spectroscopic techniques. For melting point quantification, Stuart, SMP10 (England) device was used. Bruker Kappa APEX-2 Diffractometer was used with CCD-Kamera (MoKα and graphite monochromator, = 0.71073 Å) for SC-XRD (Fig. 1–7). For NMR spectra, Bruker-Advance 300 MHz spectrometer was used with operating frequency 300 MHz for proton and 75.47 MHz for carbon. IR spectra were determined by Prestige-21 SHIMADZU Japan FTIR spectrophotometer. UV spectra were recorded on Shimadzu UV 1601 UV/Vis double beam spectrophotometer.

Synthesis of 2′,4,4″,5′-tetrafluoro-1,1':4′,1″-terphenyl (1)

Starting with 4-fluorolphenyl boronic acid (0.113 g, 0.8092 mmol), 1,4-dibromo-2,5-difluorobenzene (0.100 g, 0.3678 mmol), K_3PO_4 (0.234 g, 0.233 mmol), Pd $(PPh_3)_4$ (3 mol%, 0.013

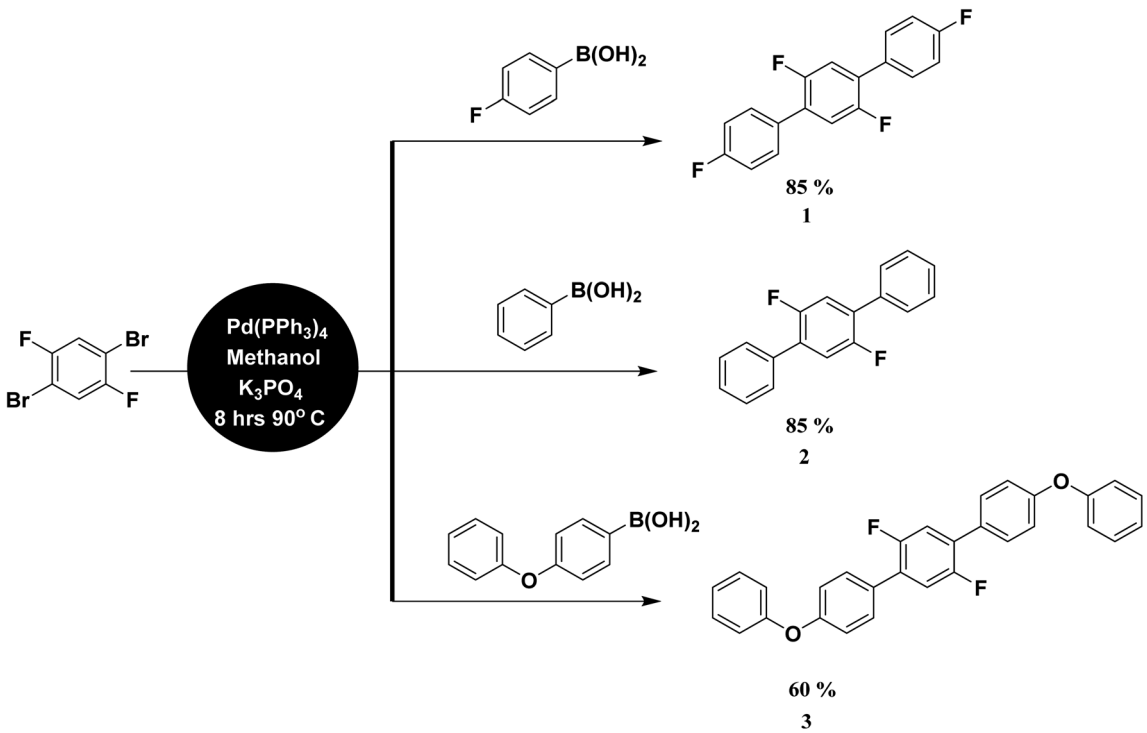

Scheme 1 General scheme for the synthesis of terphenyl compounds.

Open Access Article. Published on 17 February 2021. Downloaded on 10/26/2025 9:33:55 PM.
This article is licensed under a Creative Commons Attribution-NonCommercial 3.0 Unported Licence.

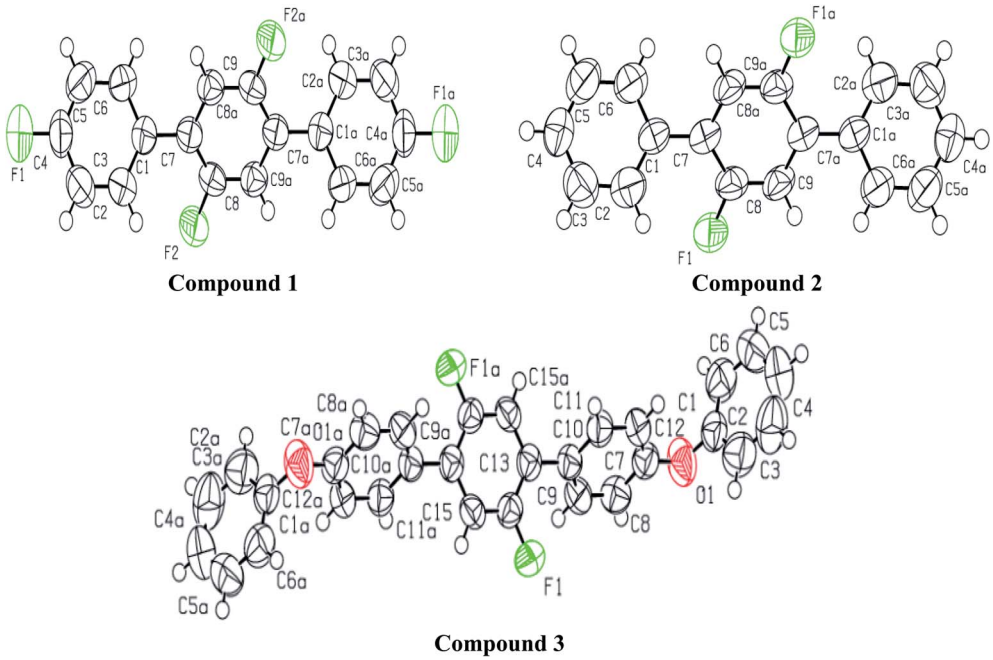

Fig. 1 ORTEP diagram of compound **1**, **2** and **3** showing the atom-labeling scheme. Displacement ellipsoids are drawn at the 50% probability level. Symmetry code: (*a*) $1-x, 1-y, -z$.

mg), in a 5 ml suspension of methanol, crystalline solid compound **1** (94 g) was synthesized and isolated with m.p 184–186 °C and yield 85%; UV λ_{max} ($CHCl_3$)/nm 339 (0.051A) (Fig. S7†). ^{1}H NMR (300 MHz, $CDCl_3$):δ = 7.70–7.65 (m, 4H, ArH), 7.59–7.57 (m, 2H, ArH), 7.27–7.23 (m, 4H, ArH), (Fig. S1†); ^{13}C NMR (75 MHz, DMSO-*d*6): δ = 161.80, 151.03, 132.16, 131.81 (C), 131.20,118.41, 116.01 (Ar-CH) (Fig. S2†); IR (KBr): ν = 1610 (w), 1525 (s), 1479 (m), 1392 (m), 1234 (br), 1163 (m), 1018 (w), 883 (m), 829 (m), 779 (s), 623 (w) cm^{-1}.

Synthesis of 2′,5′-difluoro-1,1′:4′,1″-terphenyl (2)

Starting with phenyl boronic acid (0.098 mg, 0.809 mmol), 1, 4-dibromo-2, 5-difluorobenzene (0.100 g, 0.3678 mmol), K_3PO_4 (0.234 g, 0.233 mmol), Pd $(PPh_3)_4$ (3 mol%, 0.013 mg), in a 5 ml suspension of methanol, the compound **2** was synthesized as a light brown solid (94 mg) with m.p 158–160 °C and yield 85%; UV λ_{max} ($CHCl_3$)/nm 326 (0.508A) (Fig. S8†). ^{1}H NMR (300 MHz, $CDCl_3$): δ = 7.58–7.56 (m, 2H, ArH), 7.36–7.23 (m, 10H, ArH) (Fig. S3†); ^{13}C NMR (75 MHz, DMSO-*d*6): δ = 154.80, 136.61, 131.82, (C), 129.21, 127.80, 127.61, 118.44, (Ar-CH) (Fig. S4†); IR (KBr): ν = 2918 (w), 1916 (w), 1615 (w), 1571 (w), 1545 (w), 1485 (w), 1391 (w), 1120 (M), 1137 (m), 1045 (m), 1005 (w), 947 (w), 892 (w), 845 (w), 810 (w), 735 (w), 557 (m).

Synthesis of 2′, 5′-difluro-4,4″-diphenoxy-1,1:4′,1″-terphenyl (3)

Starting with 4-phenoxyphenyl boronic acid (0.173 g, 0.809 mmol), 1,4-dibromo-2,5-difluorobenzene (0.100 g, 0.3678

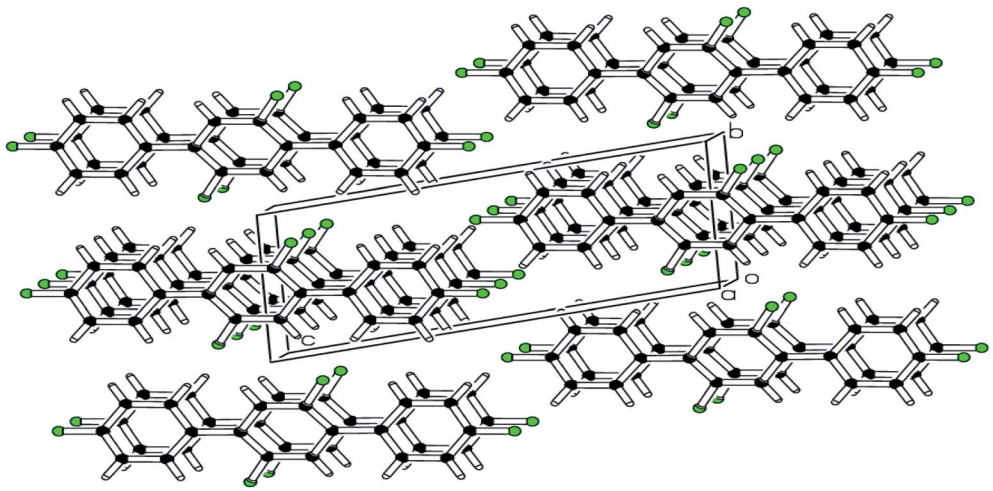

Fig. 2 pi–pi stacking stabilizing the molecules is shown in packing diagram compound **1**.

 © 2021 The Author(s). Published by the Royal Society of Chemistry

Open Access Article. Published on 17 February 2021. Downloaded on 10/26/2025 9:33:55 PM.
This article is licensed under a Creative Commons Attribution-NonCommercial 3.0 Unported Licence.

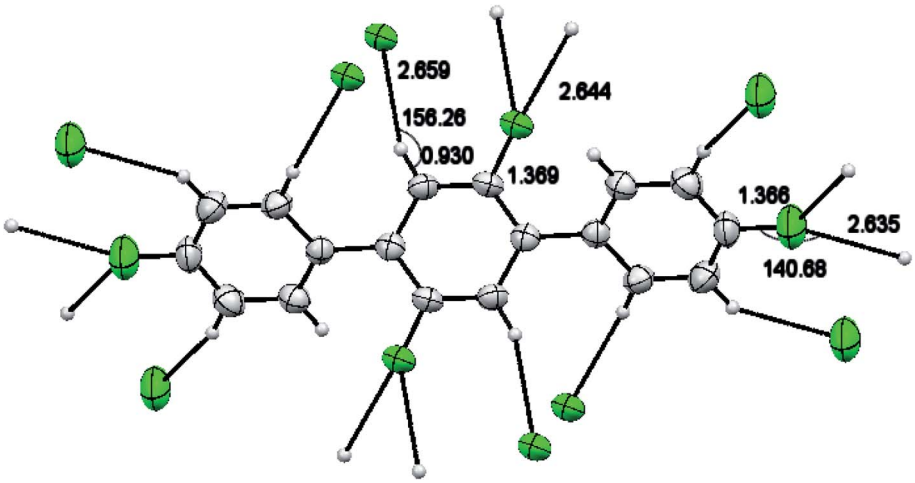

Fig. 3 CH···F and CF···H interaction in compound **1**.

mmol), K_3PO_4 (0.234 g, 0.233 mmol), Pd $(PPh_3)_4$ (3 mol%, 0.013 mg), in a 5 ml suspension of methanol, the crystalline solid compound **3** (99 mg) was synthesized with m.p 188 to 180 °C and yield 60%; UV λ_{max} ($CHCl_3$)/nm 343(1.70A) (Fig. S9†). ^{1}H NMR (300 MHz, $CDCl_3$): δ = 7.68–7.66 (m, 6H,Ar-H), 7.60–7.58 (m, 4H,Ar-H), 7.50–7.48 (m, 4H, Ar-H), 7.40–7.37 (t, 2H, Ar-H, J = 6.00 Hz), 7.27–7.23 (m, 4H, Ar-H) (Fig. S5†); ^{13}C-NMR (75 MHz, DMSO-*d*6): δ = 157.00, 155.90, 154.81, 131.11, 129.21, (C) 128.42, 121.82, 118.91, 118.40, 118.01(Ar-CH) (Fig. S6†); IR (KBr): ν = 1587 (m), 1479 (s), 1394 (w), 1230 (s), 1165 (s), 1118 (w), 889 (w), 806 (w), 785 (s), 752 (m), 690 (m), cm^{-1}.

Computational procedure

All the quantum chemical calculations in the present investigation were performed using Gaussian 16 suit of programs.[32] The geometry optimizations were performed using B3LYP with 6-311G* basis set.[33,34] The B3LYP functional is the most commonly used functional to optimize the molecular geometries for the purpose of their comparison with relevant experimental results or in combined experimental and computational studies.[35] The optimized geometries are compared with their respective experimental single crystal geometries, which showed a reasonable agreement among each other. For the calculation of linear polarizability and third-order nonlinear optical (NLO) polarizability, we used M06 functional with same 6-311G* basis set because B3LYP has been reported to overestimate the hyperpolarizabilities.[36,37] The M06 is more recently developed functional from Minnesota group of functionals as designed by Zhao and Truhlar *et al.*[38] The M06 has used to calculate NLO properties of several organic compounds. For the calculation of linear and NLO polarizabilities, we used finite field (FF) method which was originally developed by Kurtz *et al.*[39] In FF method, a static electric field is applied and NLO response properties compounds were calculated by differentiating total energy or dipole moment with respect to applied field. The details of FF methods can be found in our previous full computational studies.[40,41] For linear isotropic polarizability, the following equation was used:

$$\alpha_{\text{iso}} = \frac{1}{3}\left(\alpha_{xx} + \alpha_{yy} + \alpha_{zz}\right) \tag{1}$$

For anisotropy of linear polarizability ($\Delta\alpha$), the following equation is used:

$$\alpha_{\text{aniso}} = \frac{1}{\sqrt{2}}\sqrt{\left[\left(\alpha_{xx} - \alpha_{yy}\right)^2 + \left(\alpha_{yy} - \alpha_{zz}\right)^2 + \left(\alpha_{zz} - \alpha_{xx}\right)^2 + 6\alpha_{xz}{}^2\right]} \tag{2}$$

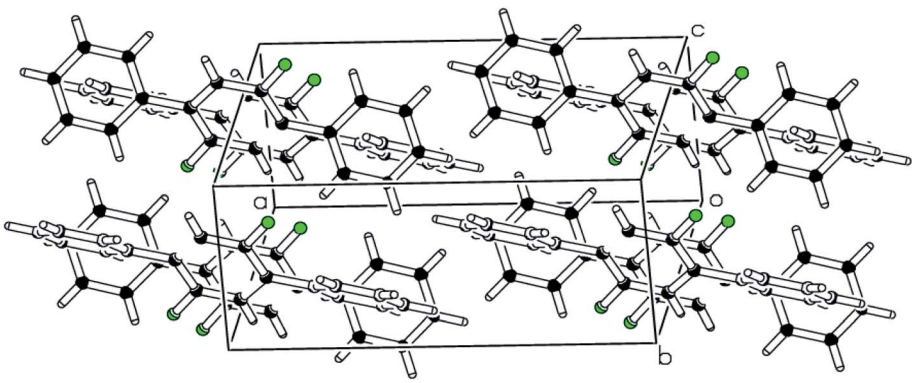

Fig. 4 pi–pi stacking along *a*-axis stabilizing the molecules is shown in packing diagram compound **2**.

Open Access Article. Published on 17 February 2021. Downloaded on 10/26/2025 9:33:55 PM.
This article is licensed under a Creative Commons Attribution-NonCommercial 3.0 Unported Licence.

Similarly, for average γ third-order polarizability:

$$\gamma = \frac{1}{15}\sum_{ij=x,y,z}\left(\gamma_{iijj} + \gamma_{ijij} + \gamma_{ijji}\right) \quad (3)$$

Under the Kleinmann symmetry, the above tensors are reduced to six components at least for static second hyperpolarizability.

$$\gamma = \frac{1}{5}\left(\gamma_{xxxx} + \gamma_{yyyy} + \gamma_{zzzz} + 2\left(\gamma_{xxyy} + \gamma_{xxzz} + \gamma_{yyzz}\right)\right) \quad (4)$$

All the individual components of polarizability and NLO optical hyperpolarizability were obtained from Gaussian 16 suit of programs.

Results and discussion

A light brown needle like crystal of the synthesized compound 2′,4,4″,5′-tetrafluoro-1,1′:4′,1″-terphenyl (**1**) $C_{18}H_{10}F_4$ was selected to get the single crystal XRD data. The approximate dimensions of crystal having triclinic system were found as $0.340 \times 0.150 \times 0.120$ mm^3. The volume of crystal was 334.63(9) Å^3. The two 4-fluoro benzene rings coupled to middle difluoro benzene ring are a bit twisted and not planar as torsion angle value of 44.1(4) ° is observed for bonds C2–C1–C7–C8. The bond length 1.492(4) Å for newly coupled C7–C1 is observed. The bond lengths 1.367(4) Å and 1.369(3) Å for bonds F1–C4 and F2–C8 were measured respectively. For C2–C1–C7 an angle of 122.0(3)°, for F2–C8–C7 an angle of 119.0(3) ° and for F1–C4–C3 an angle 118.2(3)° is observed. There is CH···F and CF···H interactions found in **1** as shown in Fig. 3. For bonds C9H9···F2; the bond length for C9–H9 is 0.930 Å and 2.659 Å for weak interaction of H9···F2 and bond angle for C9H9···F2 is 159.26°. For bonds C8F2···H9; the bond length for C8–F2 is 1.369 Å and 2.659 Å for weak interaction of H9···F2 and bond angle for C8F2···H9 is 138.14°. For bonds C4F1···H5; the bond angle is 140.68° and the bond lengths for C4–F1 and F1···H5 are 1.366 Å and 2.635 Å respectively. Different crystal parameters, refinement, bond angles and data collection are described in Table 1.

For synthesized compound 2′,5′-difluoro-1,1′:4′,1″-terphenyl (**2**) having molecular formula $C_{18}H_{12}F_2$ and F. W = 266.28, a suitable crystal having light brown color was selected. The estimated size of selected crystal was $0.320 \times 0.220 \times 0.200$ mm^3 and measured volume was 652.69(9) Å^3. The monoclinic crystal system with $P2_1/c$ was observed for compound **2** with cell dimensions as [a = 13.517(12) Å, b = 7.21(5) Å, c = 6.7331(6) Å], [α = 90°, β = 96.41(4)° and γ = 90°]. For Z = 2 and, 1.355 mg m^{-3} is the calculated density. 5080 total measured reflections and 1287 unique reflections [R(int) = 0.0346] were utilized to calculate XRD data. μ = 0.097 cm $^{-1}$ is the linear absorption coefficient. The maximum and minimum peaks and holes are

Table 1 X-ray crystallographic data of **1**, **2** and **3**[a]

Crystal parameters	**1**	**2**	**3**
CCDC #	2025097	2025098	2025099
Chemical formula	$C_{18}H_{10}F_4$	$C_{18}H_{12}F_2$	$C_{30}H_{20}F_2O_2$
M_r	302.26	266.28	450.46
Crystalsystem, space group	Triclinic, $P\bar{1}$	Monoclinic, $P2_1/c$	Monoclinic, $P2_1/n$
Temperature (K)	296	296	296
a, b, c (Å)	3.8023(6), 6.1680(10), 14.583(2)	13.5172 (12), 7.2166 (5), 6.7331 (6)	13.5116(9), 5.8650(4), 14.3546(10)
$\acute{a}$, $\hat{a}$, $\tilde{a}$ (°)	$\acute{a}$ = 98.324(10)	$\acute{a}$ = 90	$\acute{a}$ = 90
	$\hat{a}$ = 95.514(9)	$\hat{a}$ = 96.411 (4)	$\hat{a}$ = 100.463(4)
	$\tilde{a}$ = 95.661(9)	$\tilde{a}$ = 90)	$\tilde{a}$ = 90
V (Å^3)	334.63(9)	652.69 (9)	1118.62(13)
Z	1	4	2
Radiation type	Mo Kα	Mo Kα	Mo Kα
μ (mm^{-1})	0.125	0.10	0.09
Crystal size (mm)	0.340 × 0.150 × 0.120	0.32 × 0.22 × 0.20	0.42 × 0.28 × 0.22
Data collection			
Diffractometer	Bruker Kappa APEXII CCD	Bruker Kappa APEXII CCD	Bruker Kappa APEXII CCD
Absorption correction	Multi-scan (SADABS; Bruker, 2005)	Multi-scan (SADABS; Bruker, 2005)	Multi-scan (SADABS; Bruker, 2005)
T_{min}, T_{max}	0.973, 0.982	0.966, 0.974	0.965, 0.978
No. of measured, independent and observed [$I > 2\sigma(I)$] reflections	1300, 1300, 793	5080, 1287, 913	6647, 2186, 1556
R_{int}	0.000	0.035	0.051
$(\sin\theta/\lambda)_{max}$ (Å^{-1})	0.617	0.617	0.617
Refinement			
$R[F^2 > 2\sigma(F^2)]$, $wR(F^2)$, S	0.052, 0.131, 1.09	0.075, 0.227, 1.06	0.065, 0.191, 1.38
No. of reflections	2367	1287	2186
No. of parameters	148	91	155
H-atom treatment	H-atom parameters constrained	H-atom parameters constrained	H-atom parameters constrained
$\Delta\rho_{max}$, $\Delta\rho_{min}$ (e Å^{-3})	0.23, −0.20	0.66, −0.21	0.21, −0.23

[a] Computer programs: APEX2 (Bruker, 2007), SAINT (Bruker, 2007), SHELXS97 (Sheldrick, 2008), SHELXL2014/6 (Sheldrick, 2015), ORTEP-3 for Windows (Farrugia, 1997) and PLATON (Spek, 2009), WinGX (Farrugia, 1999) and PLATON (Spek, 2009).

 © 2021 The Author(s). Published by the Royal Society of Chemistry

Open Access Article. Published on 17 February 2021. Downloaded on 10/26/2025 9:33:55 PM.
This article is licensed under a Creative Commons Attribution-NonCommercial 3.0 Unported Licence.

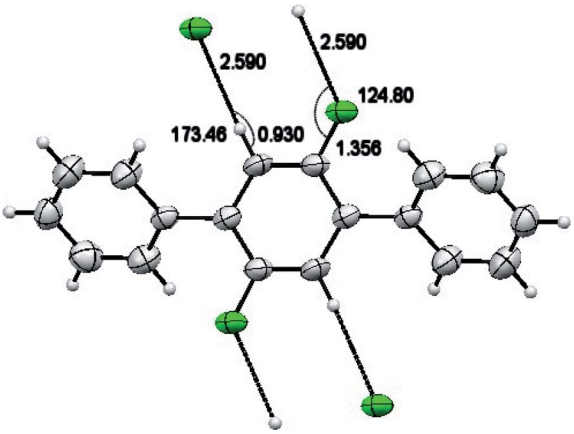

Fig. 5 CH···F and CF···H interaction in compound 2.

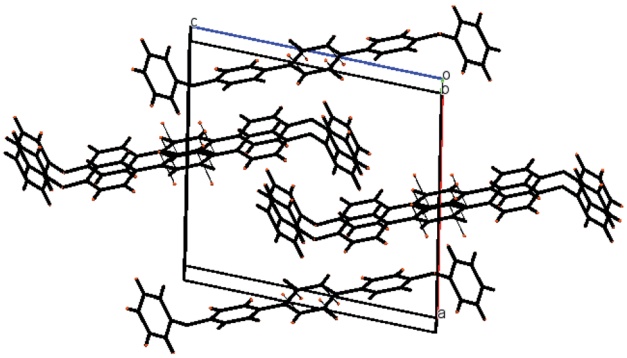

Fig. 6 The packing diagram shows that molecules are stacked with pi–pi interaction along the *a*-axis of compound 3.

0.66 and −0.21 e Å^{-3}, respectively. For bonds C2–C1–C7–C8 torsion angle value of 39.7(3)° predicts that the two aryl rings attached to middle difluoro benzene ring are a bit twisted. For C1–C7 the bond length is 1.489(3) Å. For F1–C8 and C8–C9 the bond lengths are 1.357(2) Å and 1.370(3) Å respectively. Angles of 122.43(19)°, 124.0(2)° and 120.9(2)° were observed for bonds C2–C1–C7, C8–C7–C1 and F1–C9–C7–C1 respectively. There is CH···F and CF…H interactions found in compound **2** as shown in Fig. 5. For bonds C8F1···H9; the bond angle is 124.80° and the bond lengths for C8–F1 and F1···H9 are 1.356 Å and 2.590 Å respectively. Different crystal parameters, refinement, bond angles and data collection are described in Table 1.

The molecules of 2′,5′-difluro-4,4″-diphenoxy-1,1:4′,1″-terphenyl (**3**) are symmetric. The symmetry in **3** molecules is due to a mirror plane passing through C15 and C15a atoms in the middle difluro benzene. The compound **3** molecule can be divided into three parts *i.e.* (i) **A** = the phenoxy group (PhO) (C1–C6/O1), (ii) **B** = phenyl group (Ph) (C7–C12) and (iii) **C** = difluoro benzene ring (C13–C15/C13a–C15a/F1/F1a) are not planar as they are a bit twisted. The dihedral angle between **A** and **B** is 89.93(5)°, **A** and **C** is 63.50(8)°, and **B** and **C** is 50.45(6)°. No classical H-bonds were observed in **3** molecules. The stability of compound **3** is due to F–C–F···π and π···π interactions. There is CF…C interactions found in compound **3** as shown in Fig. 7. For bonds C14–F1···C15; the bond angle is 112.10° and the bond lengths for C14–F1 and F1···C15 are 1.360 Å and 3.149 Å respectively. The packing diagram is shown in Fig. 6.

Hirshfeld analysis

Each point of the Hirshfeld surface contained two kinds of critical distances *viz* de and di, these were the distances from that point to the adjacent nucleus, outward and inward to the surface of molecule respectively.[42,43] Hirshfeld surface analysis for **1**, **2** and **3** was done to estimate the strength of intermolecular interactions. The Hirshfeld surface structure for compounds **1**, **2** and **3** are arranged in Fig. 8(A–C) respectively. According to Hirshfeld$_{norm}$ displayed a surface plot, red, white and blue colours indicated strongest, intermediate and weakest intermolecular interactions respectively.[44,45]

2-Dimensional fingerprint plots were helpful to evaluate intermolecular interactions in regard to measuring individual participation of each intermolecular interaction present in the structure.[46] The individual intermolecular interactions of compounds are plotted in Fig. 9. Percentage intermolecular contributions of different inter-atomic associations of compounds **1**, **2** and **3** surfaces are also shown in Fig. 9.

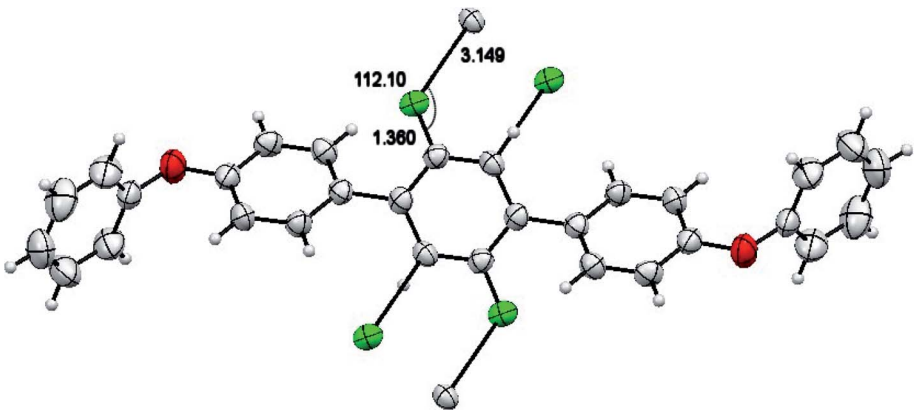

Fig. 7 CF···H interactions in compound 3.

Open Access Article. Published on 17 February 2021. Downloaded on 10/26/2025 9:33:55 PM.
This article is licensed under a Creative Commons Attribution-NonCommercial 3.0 Unported Licence.

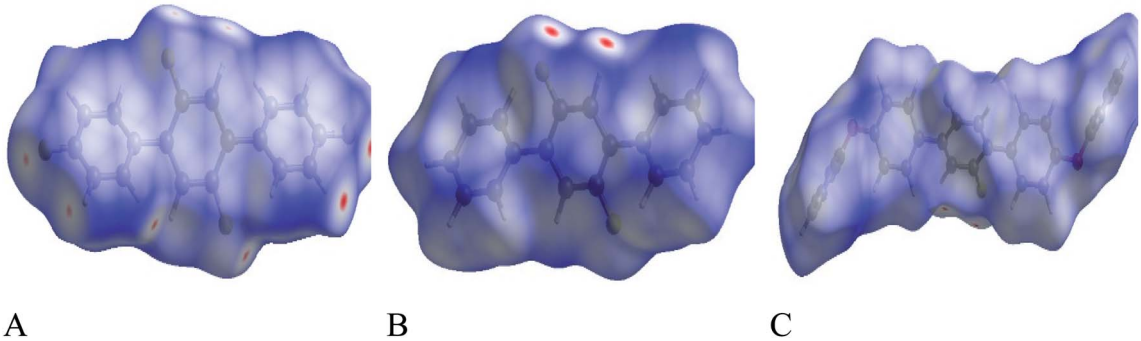

Fig. 8 (A–C) shows Hirshfeld surfaces plotted over d_{norm} in the range from −0.0596 to 1.1370, −0.0820 to 1.1006 and −0.0170 to 1.4638 a.u for compounds **1**, **2** and **3** respectively. As in electron density 1 a.u. = 6.748 e Å^{-3}.

Moreover, in the figures percentage contributions in the Hirshfeld surface concerning the outsider atoms clarifies and explain its role in crystal packing.

Geometric parameters

The optimized geometrical parameters are compared with their single crystal counterparts for compounds **1**, **2** and **3**. To make

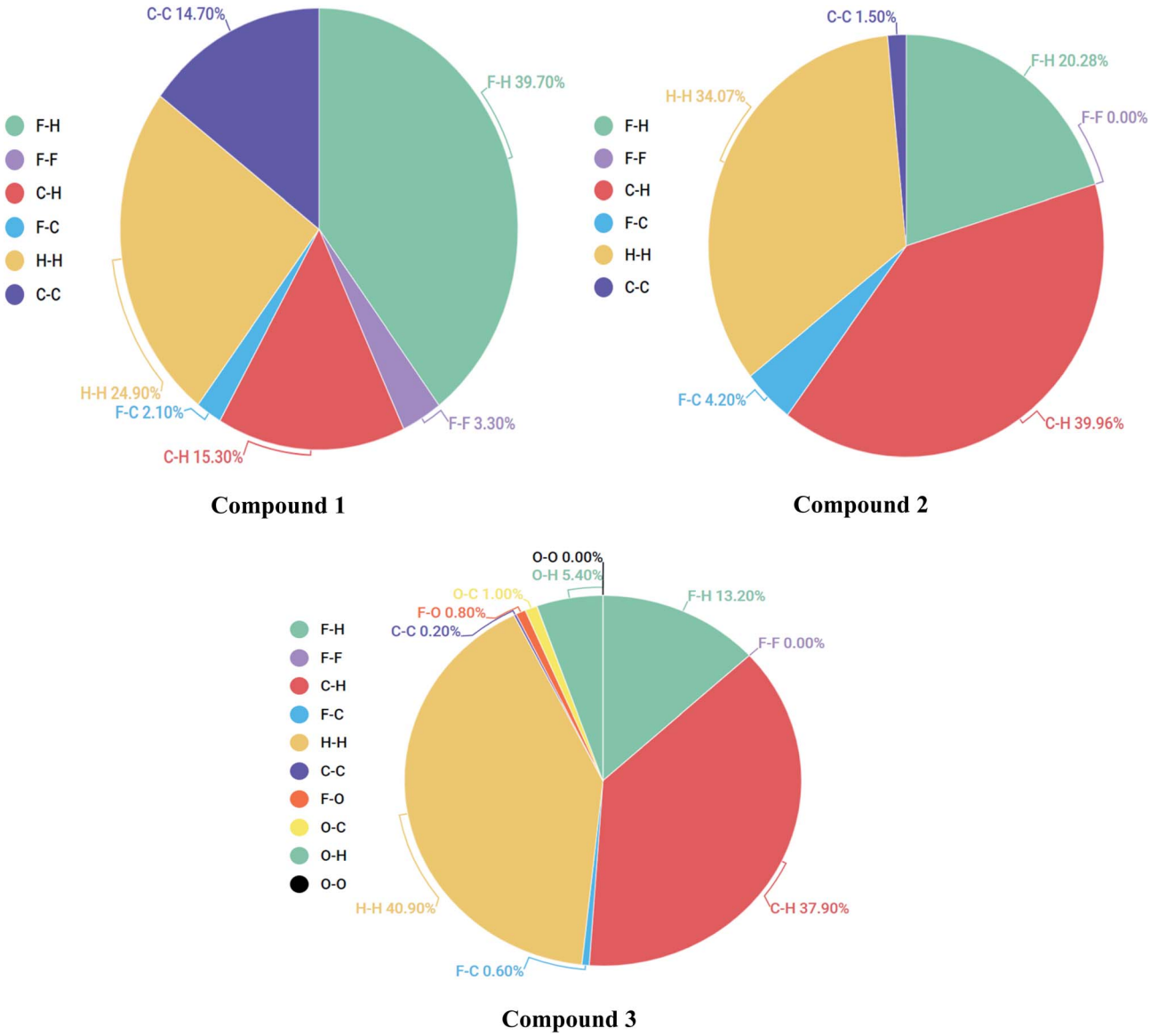

Fig. 9 Individual intermolecular interactions of compounds **1**, **2** and **3**.

 © 2021 The Author(s). Published by the Royal Society of Chemistry

Open Access Article. Published on 17 February 2021. Downloaded on 10/26/2025 9:33:55 PM.
This article is licensed under a Creative Commons Attribution-NonCommercial 3.0 Unported Licence.

geometry comparison more comprehensive, we have done the comparative analysis of important bond lengths in graphical illustration as shown in Fig. 10. The Fig. 10 shows that there is reasonably good agreement between calculated and experimental bond lengths. The bond lengths of all compounds are drawn graphical for one half only because their geometries are symmetrically arranged. The study of torsion angles shows that for compound **1** its central core difluoro-benzene ring is found somewhat non-planer to the terminal benzene rings with their calculated and experimental torsion angles (C11–C12–C13–C14) of 40.15° and 37.69°, respectively. Similar, non-planarity were also found between central core difluoro-benzene ring and their terminal groups for compounds **2** (C30–C29–C19–C30) and **3** (C44–C45–C51–C52) with their calculated (experimental) torsion angles of 40.84°(40.53°) and 41.30°(50.12°), respectively. The variations in the calculated and experimental torsion angles of compound **3** are probably due to the gas phase and solid-state geometries where larger systems cause more torsional compressions in under high pressure solid-state.

Average linear polarizability

The polarizability shows the capacity of a molecule to retort to an electric field and to attain an electric dipole moment.[47] It is noteworthy that linear polarizability also plays an important role in turning the optical activity of a compound. Therefore, average linear polarizability of compounds **1**, **2** and **3** are calculated at M06/6-311G* level of theory and collected in Table 2. We have calculated two types of average linear polarizabilities including isotropic (α_{iso}) and anisotropic (α_{aniso}) linear polarizabilities along with their individual components.

Results mentioned in Table 2 reveal that individual polarizability component along z direction (α_{zz}) contribute maximally to the average polarizability in contrast to other component along x and y directions owing to the direction of ICT along z-axis. The compound **3** has the highest value of total isotropic linear polarizability 68.25×10^{-24} esu among all studied compounds. The average isotropic polarizability value is found almost similar as 39.24×10^{-24} esu and 39.01×10^{-24} esu in compounds **1** and **2** respectively. The similar behavior is noticed in case of average anisotropic polarizability values of investigated compounds **1**, **2** and **3** where the differences among isotropic and anisotropic linear polarizabilities are found to be 1.17×10^{-24} esu, 1.24×10^{-24} esu and 7.67×10^{-24} esu, respectively for compounds **1**, **2** and **3** which indicates that direction of applied electric field does not influence the polarization process in our studied compounds.

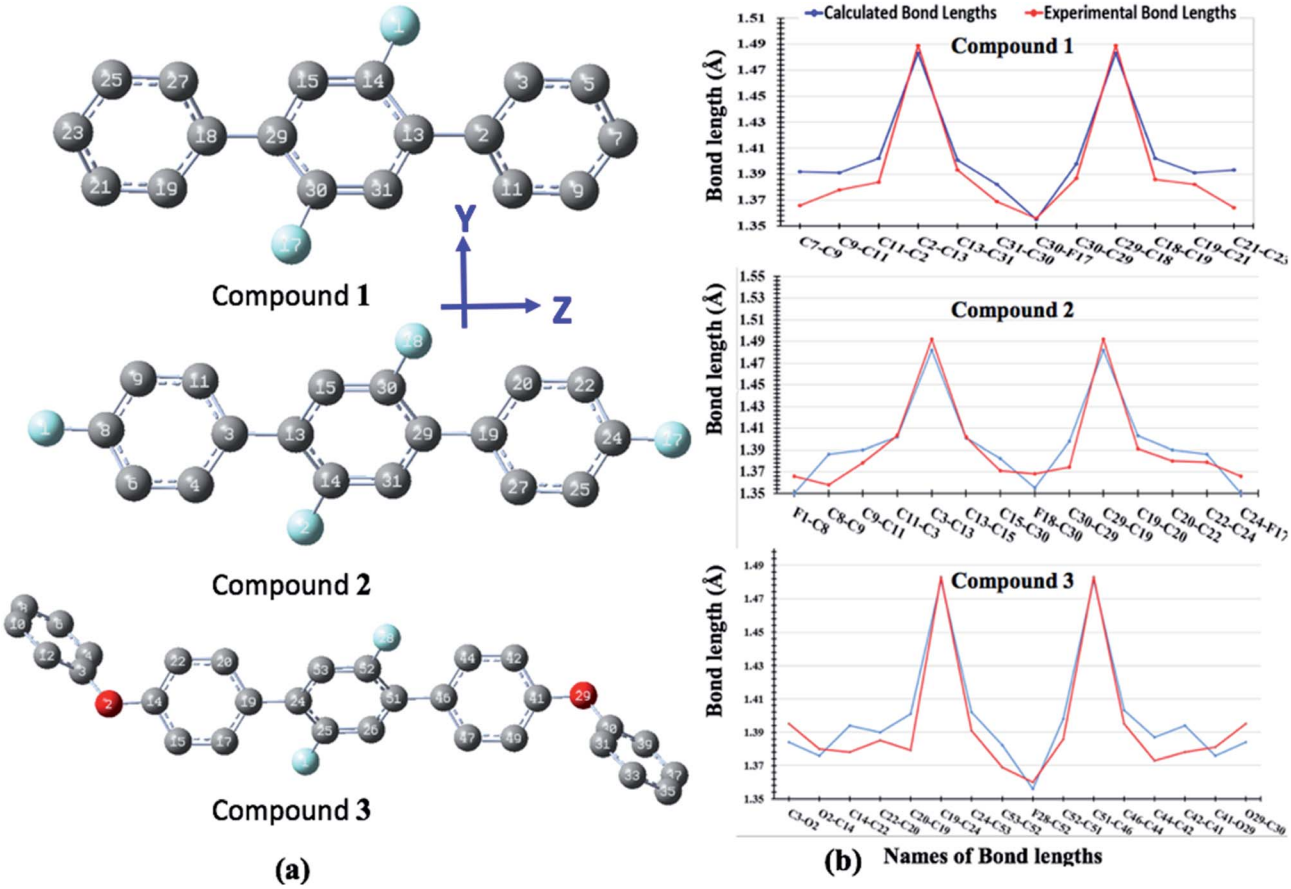

Fig. 10 The optimized geometries of compounds **1**, **2** and **3** where H-atoms are omitted for purpose of clarity (a) comparison of calculated and experimental geometrical parameters for compounds **1**, **2** and **3** (b).

Open Access Article. Published on 17 February 2021. Downloaded on 10/26/2025 9:33:55 PM.
This article is licensed under a Creative Commons Attribution-NonCommercial 3.0 Unported Licence.

Table 2 The average isotropic and anisotropic polarizabilities ($\times 10^{-24}$ esu) along with their individual components for compounds **1**, **2**, **3** and *p*-NA at M06/6-311G* levels of theory

α components	**1**	**2**	**3**
$\acute{a}_{xx}$	32.20	18.37	49.70
$\acute{a}_{xy}$	8.846	7.197	59.49
$\acute{a}_{yy}$	22.05	38.62	95.57
$\acute{a}_{xz}$	−0.312	−5.412	−8.453
$\acute{a}_{yz}$	−0.154	−4.959	23.82
$\acute{a}_{zz}$	63.47	60.05	95.57
$\acute{a}_{\mathrm{iso}}$	39.24	39.01	68.25
$\acute{a}_{\mathrm{aniso}}$	40.41	40.25	60.58

Third-order NLO polarizability

The third-order NLO polarizability plays an important role in modern days hi-tech applications. All optical switching and computing possess a fundamental process of optically-induced change in refractive index caused by third-order NLO phenomena.[48] Usually, third-order NLO polarizability is also considered as signature of two photon absorption (TPA).[49] The third-order nonlinear polarizabilities of compounds **1**, **2**, and **3** at M06 level of theory in conjunction with 6-311G* basis set. The calculated third-order nonlinear polarizability values along with individual tensors of investigated compounds **1**, **2** and **3** are given in Table 3.

It is evident from results collected in Table 3 that compound **3** has the largest average third-order NLO polarizability amplitude of 348.7 × 10^{-36} esu, while the lowest ⟨γ⟩ amplitude is calculated for compound **1** which is 131.6 × 10^{-36} esu among all studied molecules. A comparison analysis of investigated molecules indicates that the ⟨γ⟩ amplitude of compound **3** is 2.65 times larger than compound **1** and 2.59 times larger than compound **2**. We also compared the γ results of compounds **1**, **2** and **3** with *para*-nitroaniline (*p*-NA) at same level of theory. The comparison of third-order polarizability value with standard prototype NLO molecule *p*-NA is indicated by η (which is a ration between ⟨γ⟩ amplitude of studied compound to that the ⟨γ⟩ amplitude of *p*-NA) in Table 3. A careful analysis of Table 3 shows that studied compounds **1**, **2** and **3** have 13.7 times, 5.2 times and 5.17 times larger third-order polarizability value than *p*-NA value 25.45 × 10^{-36} esu as calculated at same M06/6-311G* levels of theory. The decreasing order of ⟨γ⟩ amplitudes for all studied compounds is found as: **3** > **1** > **2**. The *p*-NA molecule comparative analysis and third-order polarizability results suggest that all investigated compounds are good candidates for NLO response properties and associated applications. The NLO analysis confirmed that all studied compounds have significant NLO properties as compared to prototype standard compound which revealed their potential for technology related NLO applications.

Table 3 The calculated values of third-order polarizability γ($\times 10^{-36}$ esu) along with its individual components as for compounds **1**, **2**, **3** and *p*-NA at M06/6-311G* levels of theory[a]

γ	**1**	**2**	**3**	*p*-NA
γ_{xxxx}	8.883	1.947	16.01	0.13
γ_{yyyy}	4.091	14.13	189.6	6.87
γ_{zzzz}	642.0	511.6	724.0	128.4
γ_{xxyy}	2.684	14.49	9.046	0.38
γ_{xxzz}	−2.395	54.21	22.13	1.81
γ_{yyzz}	−1.370	38.07	375.6	−6.29
⟨γ⟩	131.6	134.6	348.7	25.45
η^a	5.17	5.20	13.70	1

[a] The η is ratio of ⟨γ⟩ amplitudes of each compound with ⟨γ⟩ of *p*-NA.

Original of third order NLO

The origin of third order NLO is usually unveil independently by using a rough approximation which directly express the value of longitudinal γ_L. In order to trace the origin of higher-order NLO polarizability, we have executed TD-DFT computations to get a better understanding about the structure-NLO property relationship. By considering the renowned three-level approximations,[50] the spectroscopic parameters are applied to understand the origin of higher-order NLO responses of the symmetric and asymmetric compounds.

$$\gamma \propto \frac{\mu_{\mathrm{eg}}^{4}}{E_{\mathrm{eg}}^{3}} + \frac{\mu_{\mathrm{e'g}}^{2}\mu_{\mathrm{eg}}^{2}}{E_{\mathrm{eg}}^{2}E_{\mathrm{e'g}}} + \frac{\mu_{\mathrm{eg}}^{2}\left(\mu_{\mathrm{ee}} - \mu_{\mathrm{gg}}\right)}{E_{\mathrm{eg}}^{3}} \tag{5}$$

where μ_{kk} and μ_{ij} are the permanent and transition dipole moments, and E_{ij} is the transition energy. The transition dipole moment is directly related with oscillator strength of vertical excitation. This so-called three-level formula is widely used experimentally and theoretically to elaborate the variations in higher-order NLO polarizabilities.[51,52] It can be perceived from the aforementioned eqn (5) that the optimal NLO response can be obtained by higher μ_{ij} and lower E_{ij} values. For the present study, TD-DFT studies have been performed using TD-M06 functional and 6-311G* basis set. Above all equations are duly noted as a rough estimation to guess the role of spectroscopic parameters in enhancing the γ amplitude. But still these approximations got noble advantage as these are used experimentally and theoretically for estimating the change in hyperpolarizability (γ) in donor and acceptor type compounds. The TD-DFT results including excitation energy (*E*), oscillator strength (f_o) and concern molecular orbital contributions for compounds **1–3** is tabulated in Table 4.

The computed TD-DFT results of compound **1** exhibited transition energy of 4.23 eV with oscillating strength of 0.97. Similarly, the transition energy and *f* of compounds **2** and **3** are found to be 4.21, 3.95 eV and oscillator strengths are found to be 0.97 and 1.49, respectively. It is seen that compound **3** has larger oscillator strength and lower transition energy that

Table 4 The calculated transition energy (Δ*E*), oscillator strength (f_o) calculated using TDDFT/M06/6-311G* levels of theory

Comp.	Δ*E* (eV)	f_o	MO contributions
1	4.23	0.97	HOMO → LUMO (96%)
2	4.21	0.97	HOMO → LUMO (96%)
3	3.95	1.49	HOMO → LUMO (96%)

 © 2021 The Author(s). Published by the Royal Society of Chemistry

Open Access Article. Published on 17 February 2021. Downloaded on 10/26/2025 9:33:55 PM.
This article is licensed under a Creative Commons Attribution-NonCommercial 3.0 Unported Licence.

results in larger amplitude of γ in compound **3** as compared with compounds **1** and **2**. Thus, the parameters of three-level approximation including transition energy and oscillator strengths were also found in line with trend ofγ amplitudes as calculated by FF method.

The γ density analysis for third-order NLO polarizability

Nakano *et al.*,[50,51] have suggested and used derivative of electron density for analyzing the spatial contributions of electrons to the third-order NLO polarizability. This 3-D depiction of the electron density derivatives is useful for illustrative spatial roles of electrons and also for revealing the electron correlation properties of higher-order polarizabilities. The γ density, defines the spatial electronic contributions to γ_{iii}value. The numerical calculation of this γ density is achieved as the third-order derivative of electron density with respect to applied electric field as given in following equation:

$$\rho_{iii}{}^{(3)}(r) = \frac{\partial^3 \rho(r)}{\partial F_i \partial F_i \partial F_i}\Big|_{F=0} \tag{6}$$

Using this density, $\gamma_{iii}$is obtained by

$$\gamma_{iii} = \frac{1}{3!}\int r_i \rho_{iii}{}^{(3)}(r)\mathrm{d}r, \tag{7}$$

where r_i signifies the i component of the position vector. A pair of positive and negative γ densities provide a description of local contributions of electrons as shown in Fig. 11. Similarly, the primary positive and negative γ densities in compounds **1**, **2** and **3** show clear distributions with larger amplitudes towards the left and right edges. Furthermore, the γ density distribution plots show that π-electrons specify the major contributions to the γ values especially in compound **3** with larger amplitudes positive and negative γ densities (see Fig. 11).

Frontier molecular orbital (FMO) analysis

Frontier molecular orbitals (FMOs) analysis offers useful insights like chemical stability, interactions between the atoms, electronic behavior and charge transfer ability of investigated compounds **1**, **2** and **3**.[53,54] The TD-DFT calculations show that HOMO and LUMO are crucial orbitals during intramolecular electronic transition process. The electronic density distributions for HOMO and LUMO orbitals are plotted as 3-D counters and shown in Fig. 12. A careful analysis of HOMO and LUMO orbital distributions in Fig. 12 illustrates that there are middling charge redistributions upon electronic transitions among compounds **1** and **2**. While on the other hands, compound **3** indicates a clear intramolecular charge transfer process (from terminal phenyl groups to central core) as seen by the delocalized distributions of its HOMO and LUMO orbitals. The eletronic transition energy of a molecular system significantly depends upon the distribution of its FMOs and their relative energies.[55] Moreover, HOMO–LUMO energy gap ($E_{\mathrm{HL}} = E_{\mathrm{LUMO}} - E_{\mathrm{HOMO}}$) is also used to calculate various global reactivity parameters. Compounds with narrow HOMO–LUMO energy gap is considered highly reactive, soft in nature with least stability.[56] Contrarily, a compound enclosing large HOMO–LUMO energy gap is marked hard in nature and less reactive with higher stability.[57] The M06/6-311G* level of theory is utilized to gain frontier molecular orbitals of investigated compounds **1**–**3**. The computed results of HOMO and LUMO energies along with energy gaps are collected in Table 5.

The energy gap values of investigated compounds **1**, **2** are **3** are found close to each other with only a little difference of 0.039 eV. However, the smallest energy gap value among all investigated compounds **1**–**3** is found in the case of **3** with ΔE_{HL} value of 4.799 eV. Overall, increasing order of ΔE_{HL} is noticed as: **3** (4.799 eV) < **2** (5.075 eV) < **1** (5.114 eV). The 3-D pictorial

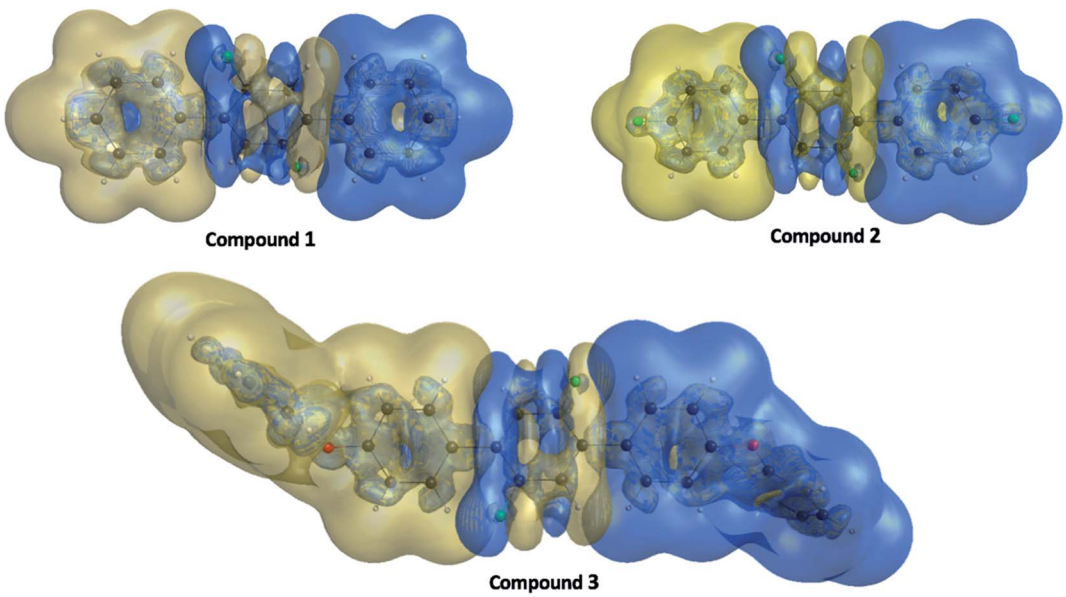

Fig. 11 The γ density $\rho_{iii}{}^{(3)}(r)$ distributions for compounds **1**, **2** and **3** where the golden and blue meshes represent positive and negative γ densities with iso-surfaces of ±10.00 a. u., respectively.

Open Access Article. Published on 17 February 2021. Downloaded on 10/26/2025 9:33:55 PM.
This article is licensed under a Creative Commons Attribution-NonCommercial 3.0 Unported Licence.

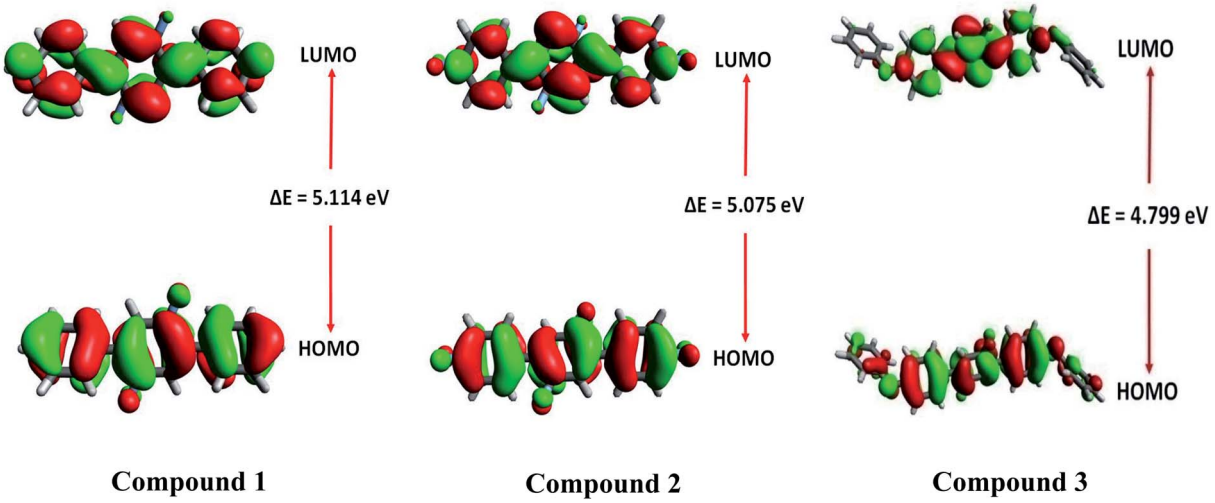

Fig. 12 Frontier molecular orbitals of 1–3.

Table 5 Frontier molecular orbitals (HOMO and LUMO) energies and energy gap values of investigated compounds 1–3

Compounds	E_{HOMO} (eV)	E_{LUMO} (eV)	ΔE_{HL} (eV)
1	−6.572	−1.458	5.114
2	−6.681	−1.606	5.075
3	−6.187	−1.388	4.799

representation of HOMO and LUMO of investigated molecules is shown in Fig. 12.

Density of states (DOS)

For the determination of contributions of electronic states of each fragment to overall molecular system, we have calculated the partial density of state (PDOS) projected to individual fragments and their total density of state (TDOS) for compounds **1**, **2** and **3** as given in Fig. 13. We have divided DOS of the compounds **1**, **2** and **3** into two fragments *i.e.* central group and terminal group as shown in Fig. 13. There are more number of states per electron volt in compound **3** as compared to compound **1** and **2** owing to the more number of atoms in compound **3**. A careful analysis of Fig. 13 shows that the central core (blue encircled fragment) is same in all the three compounds but its contributions are different in compound **3** as compared to compounds **1** and **2**. There is significant contribution of electronic states from the central core in the HOMO and LUMO orbital energy levels in compounds **1** and **2** while on the other hands, for compound **3** its PDOS shows less electronic states in HOMO and more in LUMO orbital energy levels. The trend of PDOS in compound **3** is different because there is clear push–pull configuration in compound **3** where central core is acting as electron pulling moiety while terminal fragments (methoxy-phenyl) are performing as electron pushing moieties. Thus, an intramolecular charge transfer process is envisioned from DOS studies of above entitled compounds.

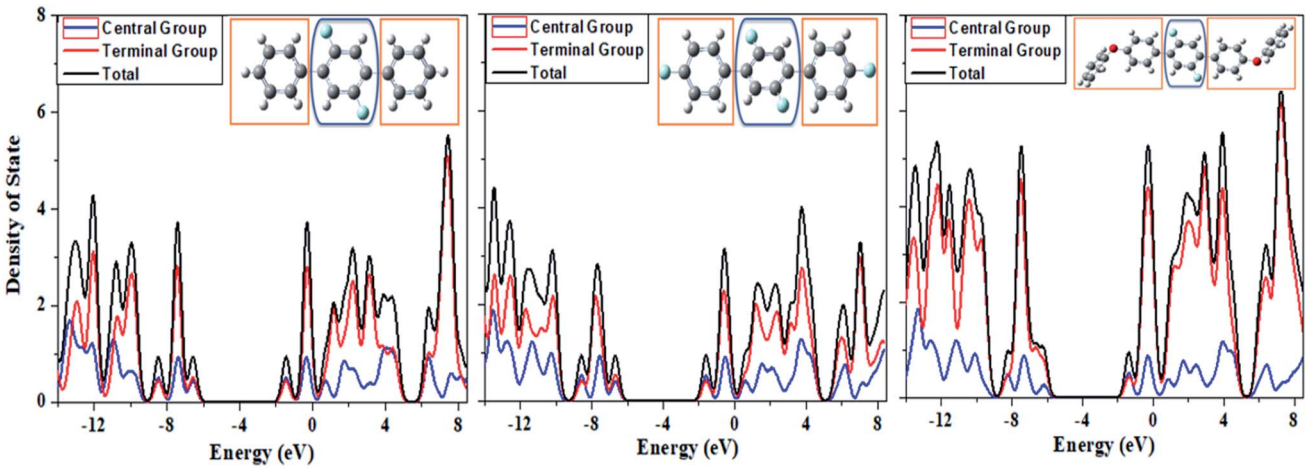

Fig. 13 The computed spectra of partial density of state (PDOS) and total density of state (TDOS) for the systems 1, 2 and 3 from left to right, respectively.

 © 2021 The Author(s). Published by the Royal Society of Chemistry

Open Access Article. Published on 17 February 2021. Downloaded on 10/26/2025 9:33:55 PM.
This article is licensed under a Creative Commons Attribution-NonCommercial 3.0 Unported Licence.

Conclusion

Three novel fluorinated terphenyl compounds *i.e.*, 2′,4,4″,5′-tetrafluoro-1,1':4′,1″-terphenyl (**1**), 2′,5′-difluoro-1,1':4′,1″-terphenyl (**2**) and 2′,5′-difluro-4,4″-diphenoxy-1,1:4′,1″-terphenyl (**3**) have been synthesized by Suzuki Miyaura approach followed by spectroscopic characterization and single crystal XRD analysis. Additionally, we applied density functional theory (DFT) methods for the calculations of third-order NLO response properties which are crucial indicators for third-harmonic generation and also often perceived as signature of two-photon absorption process. The validity of theoretical computational results has also tested by comparing experimental and computed data for synthesized compounds. The geometrical parameter of experimental SC-XRD results were closely related to optimized geometry DFT result. SC-XRD study revealed the stabilization due to pi–pi stacking in molecular packing along with F···H and F···C interaction. Hirshfeld Surface analysis explores the strength of intermolecular interactions present in compounds. Time-dependent density functional theory (TD-DFT) calculations were also performed to calculate transition energies of studied compound and the results of transition energies were used to trace the origin of third-order NLO response properties through three-level approximation. The molecular level insights were obtained by analyzing the frontier molecular orbitals (FMO) and DOS plots, which clearly projected intramolecular charge transfer process in the entitled compounds. The entitled compounds especially compound **3** showed a smaller HOMO–LUMO energy gap that suggests enhanced nonlinear optical (NLO) characteristics. To enhance the scope of our findings a semi-quantitative analysis was made by comparing of all investigated compounds with that of p-NA (often considered a prototype NLO molecule) at same methodology level. The compounds **1**, **2** and **3** have shown significant NLO properties which are about 13.7 times, 5.2 times and 5.17 times larger than that of *p*-NA (25.45×10^{-36} esu). Thus, the present investigation highlights not only synthesis compounds **1**, **2** and **3** but also highlight their computational exploration as advanced functional materials.

Conflicts of interest

There are no conflicts to declare.

Acknowledgements

The author from King Khalid University extends his appreciation to Deanship of Scientific Research at King Khalid University for funding the work through Research Project (R.G.P.2/109/41).

References

1 Z. Peng and L. Yu, *Macromolecules*, 1994, **27**, 2638–2640.
2 N. Tsutsumi, M. Morishima and W. Sakai, *Macromolecules*, 1998, **31**, 7764–7769.
3 E. M. Breitung, C.-F. Shu and R. J. McMahon, *J. Am. Chem. Soc.*, 2000, **122**, 1154–1160.
4 C.-C. Chang, C.-L. Pai, W.-C. Chen and S. A. Jenekhe, *Thin Solid Films*, 2005, **479**, 254–260.
5 M. G. Papadopoulos, A. J. Sadlej and J. Leszczynski, *Nonlinear optical properties of matter, Springer*, 2006.
6 R. W. Munn and C. Ironside, *Principles and applications of nonlinear optical materials, Springer*, 1993.
7 K. Rottwitt and P. Tidemand-Lichtenberg, *Nonlinear optics: principles and applications*, CRC Press, 2014.
8 P. S. Halasyamani and W. Zhang, *Inorg. Chem.*, 2017, **56**, 12077–12085.
9 B. Zhang, G. Shi, Z. Yang, F. Zhang and S. Pan, *Angew. Chem., Int. Ed.*, 2017, **56**, 3916–3919.
10 S. Yamashita, *J. Lightwave Technol.*, 2012, **30**, 427–447.
11 L. Guo, Z. Guo and X. Li, *J. Mater. Sci. Mater. Electron.*, 2018, **29**, 2577–2584.
12 R. Mahmood, M. R. S. A. Janjua and S. Jamil, *J. Cluster Sci.*, 2017, **28**, 3175–3183.
13 P. N. Prasad and D. J. Williams, *Introduction to nonlinear optical effects in molecules and polymers*, Wiley, New York, 1991.
14 H. Nalwa, S. Miyata and P. A. Fleitz, *Opt. Eng.*, 1997, **36**, 2622.
15 F. Bureš, D. Cvejn, K. Melánová, L. Beneš, J. Svoboda, V. Zima, O. Pytela, T. Mikysek, Z. Růžičková and I. Kityk, *J. Mater. Chem. C*, 2016, **4**, 468–478.
16 A. Karakas, T. Dag, H. El Ouazzani, K. Sebiaai and Y. Boughaleb, *Opt. Quant. Electron.*, 2014, **46**, 165–170.
17 L. Kamath, K. Manjunatha, S. Shettigar, G. Umesh, B. Narayana, S. Samshuddin and B. Sarojini, *Optic Laser. Technol.*, 2014, **56**, 425–429.
18 Y. S. Mary, C. Y. Panicker, B. Narayana, S. Samshuddin, B. Sarojini and C. Van Alsenoy, *Spectrochim. Acta, Part A*, 2014, **133**, 480–488.
19 H.-R. Liao, Y.-J. Lin, Y.-M. Chou, F.-T. Luo and B.-C. Wang, *J. Lumin.*, 2008, **128**, 1373–1378.
20 J. Hou, C. Yang, J. Qiao and Y. Li, *Synth. Met.*, 2005, **150**, 297–304.
21 K. Colladet, M. Nicolas, L. Goris, L. Lutsen and D. Vanderzande, *Thin Solid Films*, 2004, **451**, 7–11.
22 C. D. Dimitrakopoulos and P. R. Malenfant, *Adv. Mater.*, 2002, **14**, 99–117.
23 R. Friend, R. Gymer, A. Holmes, J. Burroughes, R. Marks, C. Taliani, D. Bradley, D. Dos Santos, J. Bredas and M. Lögdlund, *Nature*, 1999, **397**, 121–128.
24 B. A. Reinhardt, L. L. Brott, S. J. Clarson, A. G. Dillard, J. C. Bhatt, R. Kannan, L. Yuan, G. S. He and P. N. Prasad, *Chem. Mater.*, 1998, **10**, 1863–1874.
25 J.-K. Liu, *Chem. Rev.*, 2006, **106**, 2209–2223.
26 D. N. Quang, T. Hashimoto, M. Nukada, I. Yamamoto, M. Tanaka and Y. Asakawa, *Planta Med.*, 2003, **69**, 1063–1066.
27 S.-Z. Tian, X. Pu, G. Luo, L.-X. Zhao, L.-H. Xu, W.-J. Li and Y. Luo, *J. Agric. Food Chem.*, 2013, **61**, 3006–3012.
28 J. Qiu, B. Zhao, W. Zhong, Y. Shen and H. Lin, *Eur. J. Med. Chem.*, 2015, **94**, 427–435.

Open Access Article. Published on 17 February 2021. Downloaded on 10/26/2025 9:33:55 PM.
This article is licensed under a Creative Commons Attribution-NonCommercial 3.0 Unported Licence.

29 A. Kamal, M. K. Reddy, T. B. Shaik, Y. Srikanth, V. S. Reddy, G. B. Kumar and S. V. Kalivendi, *Eur. J. Med. Chem.*, 2012, **50**, 9–17.
30 A. Parish, S. Gauza, S. T. Wu, J. Dziaduszek and R. Dabrowski, *Liq. Cryst.*, 2008, **35**, 79–86.
31 A. Parish, S. Gauza, S.-T. Wu, J. Dziaduszek and R. Dabrowski, *Mol. Cryst. Liq. Cryst.*, 2008, **489**, 22/[348]–339/[365].
32 M. J. Frisch, G. W. Trucks, H. B. Schlegel, G. E. Scuseria, M. A. Robb, J. R. Cheeseman, G. Scalmani, V. Barone, G. A. Petersson, H. Nakatsuji, X. Li, M. Caricato, A. V. Marenich, J. Bloino, B. G. Janesko, R. Gomperts, B. Mennucci, H. P. Hratchian, J. V. Ortiz, A. F. Izmaylov, J. L. Sonnenberg, D. Williams-Young, F. Ding, F. Lipparini, F. Egidi, J. Goings, B. Peng, A. Petrone, T. Henderson, D. Ranasinghe, V. G. Zakrzewski, J. Gao, N. Rega, G. Zheng, W. Liang, M. Hada, M. Ehara, K. Toyota, R. Fukuda, J. Hasegawa, M. Ishida, T. Nakajima, Y. Honda, O. Kitao, H. Nakai, T. Vreven, K. Throssell, J. A. Montgomery Jr, J. E. Peralta, F. Ogliaro, M. J. Bearpark, J. J. Heyd, E. N. Brothers, K. N. Kudin, V. N. Staroverov, T. A. Keith, R. Kobayashi, J. Normand, K. Raghavachari, A. P. Rendell, J. C. Burant, S. S. Iyengar, J. Tomasi, M. Cossi, J. M. Millam, M. Klene, C. Adamo, R. Cammi, J. W. Ochterski, R. L. Martin, K. Morokuma, O. Farkas, J. B. Foresman and D. J. Fox, *Gaussian 16 Rev. B.01*, 2016.
33 A. D. Becke, *J. Chem. Phys.*, 1993, **98**, 1372–1377.
34 C. Lee, W. Yang and R. G. Parr, *Phys. Rev. B: Condens. Matter Mater. Phys.*, 1988, **37**, 785.
35 M. M. Jadhav, T. H. Chowdhury, I. Bedja, D. Patil, A. Islam and N. Sekar, *Dyes Pigm.*, 2019, **165**, 391–399.
36 A. G. Ioannou, S. M. Colwell and R. D. Amos, *Chem. Phys. Lett.*, 1997, **278**, 278–284.
37 S. Muhammad, A. R. Chaudhry and A. G. Al-Sehemi, *Optik*, 2017, **147**, 439–445.
38 Y. Zhao and D. G. Truhlar, *Theor. Chem. Acc.*, 2008, **120**, 215–241.
39 H. A. Kurtz, J. J. Stewart and K. M. Dieter, *J. Comput. Chem.*, 1990, **11**, 82–87.
40 S. Muhammad, *J. Mol. Graphics Modell.*, 2015, **59**, 14–20.
41 S. Muhammad, *Mater. Chem. Phys.*, 2018, **220**, 286–292.
42 A. D. Herrera-Espana, J. Aguilera-González, G. J. Mena-Rejón, S. Hernández-Ortega and D. Cáceres-Castillo, *Acta Crystallogr., Sect. E: Crystallogr. Commun.*, 2019, **75**, 717–720.
43 N. K. Sebbar, B. Hni, T. Hökelek, A. Jaouhar, M. Labd Taha, J. T. Mague and E. M. Essassi, *Acta Crystallogr., Sect. E: Crystallogr. Commun.*, 2019, **75**, 721–727.
44 M. A. Spackman, J. J. McKinnon and D. Jayatilaka, *CrystEngComm*, 2008, **10**, 377–388.
45 V. Nagaveni, S. Naveen, T. S. Kumar, M. Kumara, K. Mahadevan and N. Lokanath, *Pharma Chem.*, 2016, **8**, 392–396.
46 A. Saeed, M. Bolte, M. F. Erben and H. Pérez, *CrystEngComm*, 2015, **17**, 7551–7563.
47 M. U. Khan, M. Khalid, M. Ibrahim, A. A. C. Braga, M. Safdar, A. A. Al-Saadi and M. R. S. A. Janjua, *J. Phys. Chem. C*, 2018, **122**, 4009–4018.
48 J.-L. Bredas, C. Adant, P. Tackx, A. Persoons and B. Pierce, *Chem. Rev.*, 1994, **94**, 243–278.
49 G. S. He, J. Zhu, A. Baev, M. Samoć, D. L. Frattarelli, N. Watanabe, A. Facchetti, H. Ågren, T. J. Marks and P. N. Prasad, *J. Am. Chem. Soc.*, 2011, **133**, 6675–6680.
50 M. Nakano, M. Okumura, K. Yamaguchi and T. Fueno, *Mol. Cryst. Liq. Cryst.*, 1990, **182**, 1–15.
51 M. Nakano, K. Yamaguchi and T. Fueno, *Chem. Phys. Lett.*, 1991, **185**, 550–554.
52 S. Muhammad, K. Fukuda, T. Minami, R. Kishi, Y. Shigeta and M. Nakano, *Chem. - Eur. J.*, 2013, **19**, 1677–1685.
53 M. N. Arshad, A.-A. M. Al-Dies, A. M. Asiri, M. Khalid, A. S. Birinji, K. A. Al-Amry and A. A. Braga, *J. Mol. Struct.*, 2017, **1141**, 142–156.
54 M. N. Tahir, M. Khalid, A. Islam, S. M. A. Mashhadi and A. A. Braga, *J. Mol. Struct.*, 2017, **1127**, 766–776.
55 J. Wu, S.-X. Liu, A. Neels, F. Le Derf, M. Sallé and S. Decurtins, *Tetrahedron*, 2007, **63**, 11282–11286.
56 J.-i. Aihara, *J. Phys. Chem. A*, 1999, **103**, 7487–7495.
57 I. Khan, M. Khalid, M. Adeel, M. U. Khan, M. S. Khan, N. Ahmad, A. Ali and M. Akram, *Optik*, 2020, **219**, 165285.

 © 2021 The Author(s). Published by the Royal Society of Chemistry